ISSN 0024-9521
IJG Vol. 40, No. 2, December 2008 (133-152)

INDONESIAN JOURNAL OF GEOGRAPHY

APPLICATION OF REMOTE SENSING TO ESTIMATE ABOVE GROUND BIOMASS IN TROPICAL FORESTS OF INDONESIA

Arief Wijaya
Arief.Wijaya@student.tu-freiberg.de
Richard Gloaguen
Remote Sensing Group, Institute for Geology, TU-Bergakademie,

Hermann Heilmeier
Interdisciplinary Ecological Centre, Biology/Ecology

ABSTRACT

This work aims to estimate Above Ground biomass (AGB) of a tropical rainforest in East Kalimantan, Indonesia using equation derived from the stand volume prediction and to study the spatial distribution of AGB over a forest area. The potential of remote sensing and field measurement data to predict stand volume and AGB were studied. Landsat ETM data were atmospherically corrected using Dark Object Subtraction (DOS) technique, and topographic corrections were conducted using C-correction method. Stand volume was estimated using field data and remote sensing data using Levenberg-Marquardt neural networks. Stand volume data was converted into the above ground biomass using available volume – AGB equations. Spatial distribution of the AGB and the error estimate were then interpolated using kriging. Validated with observation data, the stand volume estimate showed integration of field measurement and remote sensing data has better prediction than the solitary uses of those data. The AGB estimate showed good correlations with stand volume, number of stems, and basal area.

Keywords: above ground biomass, stand volume, remote sensing, neural networks, kriging

INTRODUCTION

Tropical rainforests are the largest ecosystems and inhabit most biodiversity in the world, comprising more than half of all the world plant and animal species. However, tropical rainforests cover less than 6% of land surface on the earth nowadays. Tropical rainforests have an important role for global carbon cycle as they store ca. 30% of all terrestrial carbon (up to 200 Mg/ha) and sequester about 12 Mg/ha per year, i.e. 22% of all carbon fixed on Earth. In environmental study, biomass assessment is important for many purposes, such as resource use and

environmental management. The amount of carbon sequestered can be inferred from the biomass change since 50% of the forest dry biomass is carbon [*Losi et al.*, 2003] There are three approaches to mapping biomass in forest areas, which are field measurement, remote sensing, and GIS-based approaches [*Lu*, 2006]. The field measurement is the most accurate way to assess biomass, but it is very costly and time consuming because a destructive sampling is required [*deGier*, 2003]. Remote sensing is probably the most feasible alternative to assess forest biomass over a large area. Remote sensing becomes more popular for different applications, including for biomass assessment. Recent remote sensing studies have explored the potential of optical satellite [*Foody* and *Cox*, 1994; *Houghton et al.*, 2001; *Lu et al.*, 2004], LIDAR data [*Lefsky et al.*, 2002], or radar data [*Austin et al.*, 2003; *Rauste*, 2005] for estimating forest biomass. Those studies as well as other references on forest biomass mostly addressed the problems on the tropical rainforests of Amazon, while this study focused in tropical forest region in Central Indonesia. In his study, *Foody et al.* [2003] concluded the transferability of biomass model, which was estimated using remote sensing data still remains a challenging task. Those studies as well as this present study focused on the assessment of above ground biomass (AGB).

Remote sensing based estimation requires field data for developing biomass predictive model or for validation purpose. In the case the field data is unavailable; the biomass can be approached from stand (i.e. tree) parameters, such as tree height and stand diameter, estimated using statistical method [*Houghton et al.*, 2001; *Rahman et al.*, 2005]. *Sales et al.* [2007] predicted the forests biomass using the estimate of stand volume and statistical multi-regression method. Unlike those studies, the present study implements a non-statistical method based on artificial neural networks to predict stand volume, using which the biomass is subsequently estimated.

This study combines field measurement, digital elevation model (DEM), spectral data, and vegetation indices for predicting the stand volume. This combination certainly violates normality assumption that is required for most parametric method, thus an alternative approach using neural networks approach was applied, as it has potential to improve the accuracy of stand volume estimate. The AGB was estimated from the conversion of stand volume using two models proposed by [*Brown* and *Lugo*, 1992; *Fearnside*, 1997]. Few references conducting study in Indonesian forests to assess the biomass, especially those combining field measurement and remote sensing data, has also motivated this study.

This study focuses on a tropical rainforests located in Labanan Concession, Berau Municipality, East Kalimantan Province, Indonesia (Fig. 1). This region geographically is situated along the equator at the coordinate of 1° 45' to 2° 10' N, and 116° 55' to 117° 20' E and has a size of 83,000 hectares. The forest area is

situated in a relatively flat region with the elevation from 50 - 650 meters above sea level and enjoys annual rainfall rate of more than 1000 mm.

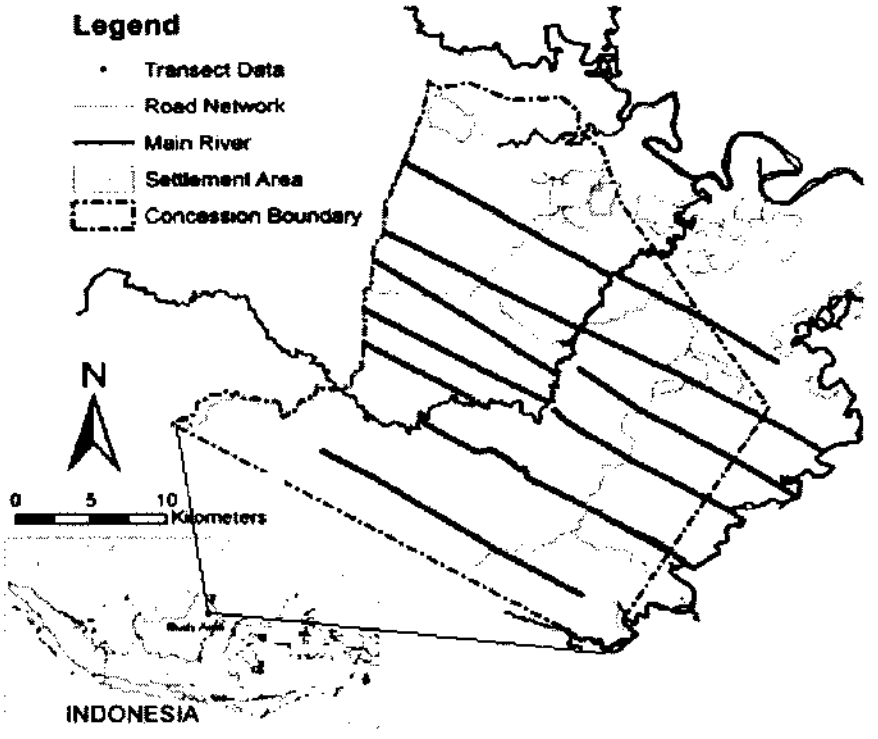

Figure 1. Boundary of Labanan Concession Forest

The forest area belongs to a state owned timber concession-holder company where active timber harvesting is carried out. The concession area is mainly situated on inland of coastal swamps and formed by undulating to rolling plains with isolated masses of high hills and mountains. The variation in topography is a consequence of folding and uplift of rocks, resulting from tension in the earth crust. The landscape of Labanan is classified into flat land, sloping land, steep land, and complex landforms, while the forest type is often called as lowland mixed dipterocarp forest [*Mantel*, 1998]. The forest covers in the area are mainly dominated with primary forest and mature secondary forest regenerated from the first cycle of timber harvesting, recently logged over forest, riparian forest with complex vegetation structure, shrubs and also agricultural and settlement areas.

THE METHODS

There were 1515 sampling plots (with average size 225 m^2) divided into 17 transect collected for forest inventory purpose and made available for this study.

The measurement was carried out on a circular nested plot with respect to tree diameter size. Trees with diameter at breast height (DBH) > 50 cm were measured up to 0.125 samples per hectare, and within this plot smaller subplots were estimated and physical properties of smaller trees were measured. The trees with DBH of 20 – 49 cm and the trees with DBH of 10 – 19 cm were measured with the sampling intensity of 0.04 sample/ha and 0.0125 sample/ha, respectively. Besides tree properties, namely DBH (cm) and number of stems per plot, the coordinate, slope and aspect of each sampling plot were also recorded. Thus, the DBH were converted into basal area per hectare; considering adjustment factors of each tree species, the actual stand volume per hectare was estimated.

Landsat 7 ETM+ image with 30 meter resolution was used for prediction of stand volume together with field measurement data (i.e. number of stems in a sample plot). The Landsat data was acquired on May 31, 2003 under a very clear atmospheric condition with almost no significant haze and cloud. The satellite image was projected using Universal Transverse Mercator (UTM) and WGS 84 datum. Preprocessing of the image was conducted for correcting atmospheric and topographic effects, since vegetation indices were computed from the radiometrically calibrated image. Digital Elevation Modeling (DEM) of the same area was obtained from Shuttle Radar Topography Mission (SRTM) data. The DEM which originally has 90 meter resolution was resampled into 30 meter resolution to fit with the spatial resolution of Landsat image; thus slope angle and aspect were computed from the resampled DEM and applied as ancillary data for stand volume prediction.

Radiometric calibration is a multi-step process that involves the use of standard equations to convert 8-bit satellite-quantized calibrated digital numbers (DN) to at-satellite reflectance. Landsat 7 images were converted to at-satellite radiance using Eq.(1),

$$L_{sat} = \left({(Lmax_{sat} - Lmin_{sat})}/{(DNmax - DNmin)} \right) \times (DN - DNmin) + Lmin_{sat} \quad \ldots\ldots\ldots (1)$$

where $Lmax_{sat}$ is band-specific spectral radiance scaled to *DNmax* (W m^{-2} sr^{-1} μm^{-1}), $Lmin_{sat}$ is band-specific spectral radiance scaled to *DNmin* (W m^{-2} sr^{-1} μm^{-1}), *DNmax* is maximum quantized calibrated digital number (255), and *DNmin* is minimum quantized calibrated digital number (0 for LPGS data, 1 for NLAPS and EOS data). Eq. (1) accounts for gain state (i.e. high/low settings) by using respective published *Lmax* and *Lmin* values as published in Landsat 7 Science Data User Handbook [*Landsat Project Science Office*, 1998].

Converting to at-satellite radiance, each Landsat band was converted into top-of-atmosphere reflectance (ρ_{TOA}) using following equation [*Lu et al.*, 2004]

$$\rho_{TOA} = \frac{\pi . d^2 . L_{sat}}{E_{sun} . cos(\theta)} \quad \text{.....(2)}$$

where d^2 is square of the earth-sun distance in astronomical units (AU) that can be found in Landsat 7 Science Data User Handbook [*Landsat Project Science Office*, 1998], E_{sun} is mean solar exo-atmospheric irradiance (W m^{-2} μm^{-1}), and θ is sun zenith angle.

The conversion from at-satellite radiance to top-of-atmosphere reflectance is known as partial correction case since by definition this value does not remove atmospheric effects due to atmospheric scattering.

For absolute atmospheric correction case, the at-satellite radiance is converted to surface reflectance (ρ), assuming a uniform Lambertian surface under cloudless condition, using following formula [*Chavez Jr.*, 1996]

$$\rho = \frac{\pi . d^2 . (L_{sat} - L_p)}{T_v . (E_{sun} . cos(\theta) . T_z + E_{down})} \quad \text{.....(3)}$$

where Lp is path radiance (W m^{-2} sr^{-1} μm^{-1}) or so-called haze layer [*Chavez Jr.*, 1988], T_v is atmospheric transmittance from the target toward the sensor, T_z is atmospheric transmittance in the illumination direction, and E_{down} is downwelling diffuse irradiance (W m^{-2} μm^{-1}). The output of atmospheric correction is the percentage of surface reflectance. There are different variations of DOS technique according to a study conducted by [*Song et al.*, 2001]. This study initially adopted two variations of DOS technique, which are DOS1 and DOS2. We found afterwards that DOS2 yields better correction results in terms of the spectral response of corrected image in relation with the actual spectral of vegetation types. Thus, hereafter the satellite image was corrected using DOS2 technique.

In order to correct topographic effects of the satellite data, Digital Elevation Model (DEM) should be assigned. The DEM should be firstly geo-referenced in the same coordinate system as the satellite image to be corrected and the DEM should also be of a scale that is close to that of the satellite image, so that the slope angle and aspect can be derived for each pixel position of the satellite image. Thus, the DEM is also used to compute the incident angle (γ_i), defined as the angle between the normal to the ground and the sun rays [*Riano et al*, 2003]. The γ_i parameters varies from -1.0 to +1.0, and are computed as:

$$\cos\gamma_i = \cos\theta_p \cos\theta_z + \sin\theta_p \sin\theta_z \cos[(\emptyset]_a - \emptyset_o) \quad \text{.....(4)}$$

where θ_p is the slope angle; θ_z is the solar zenith angle; $\emptyset_a$ is the solar azimuth angle; and $\emptyset_o$ is the aspect angle; each angle should firstly be converted into radian.

Thus, the incident angle was estimated for the whole image and the topographic correction can be carried out using different methods. A simple method to correct terrain slope in areas that receive direct solar illumination is simply to adopt Lambertian assumption (i.e. a surface reflects radiation in a diffuse fashion, so that it appears equally bright from all feasible observation angles). Instead applying terrain correction with Lambertian assumption, this study is more cautious of diffuse irradiance since most rugged terrains basically have a non-Lambertian behavior. This non-Lambertian correction models include Minnaert correction [*Minnaert*, 1941], which is probably the most popular empirical method for computing a complicated Bidirectional Reflectance Distribution Function (BRDF) of rugged terrain areas. This study however implemented another empirical-statistical method assuming a linear correlation between the reflectance of each satellite band under an inclined surface (ρ_T) and the incident angle cosine ($\cos \gamma_i$) as [*Teillet et al.*, 1982].

$$\rho_T = b_k + m_k \cdot \cos \gamma_i \quad \ldots\ldots (5)$$

where m_k is the slope of the regression line for band k. The b_k is considered constant for the entire image, being the intercept in the regression equation. A variation of this empirical approach is called the C-correction method [*Teillet et al.*, 1982] and the correction of the ρ_T is defined as

$$\rho_H = \rho_T \left[\frac{\cos \theta_z + \left(b_k / m_k \right)}{\cos \gamma_i + \left(b_k / m_k \right)} \right] \quad \ldots\ldots (6)$$

where θ_z is the solar zenith angle, and ρ_H is the reflectance of a horizontal surface.

Stand volume estimate

The utility of neural networks to estimate forest properties is based on the assumption that this method, unlike conventional parametric approaches, does not need a normality assumption [*Cohen* and *Cohen*, 1983]. Field measurement, spectral data, DEM and vegetation indices clearly have different nature of data distribution, thus combining these data commonly violates the normal distribution assumption. The conventional multi-linear regression method has a limitation to predict such data as this method is bounded by a normality assumption [*Berry* and *Fedlman*, 1985]. The study of comparison on prediction ability between neural networks and multi-linear regression has been conducted in different applications, such as medical and pharmaceutical technology [*Sathe* and *Venitz*, 2003], environmental modeling [*Baik* and *Peak*, 2000; *Sousa et al.*, 2007], chemistry and material science [*Bolanca et al.*, 2005], and marketing and business [*Lim* and *Kirikoshi*, 2005]. These studies found that neural networks have performed better than multi-linear regression for the prediction using a more complex input data variation.

The neural networks basically works based on the interconnected neurons [*Wijaya*, 2006]. The neuron sums up the weighing of the input value and applies a threshold function to such value. This process, so called training process, most of the time is very time consuming, so that to make the training process faster a training algorithm should be considered. There are different algorithms which can be used for training the neural networks. The back-propagation algorithm is probably the most famous training algorithm for the neural networks [*Atkinson* and *Tatnall*, 1997]. Nevertheless this algorithm needs the proper parameters in order to give a reasonable result. Based on our experience the training using back-propagation method is time expensive as it requires a large number of training iterations to find an optimal solution.

In contrast with other studies, this work implemented Levenberg-Marquardt algorithm for training a feed-forward neural networks [*Hagan* and *Menhaj*, 1994]. Experiments with the Levenberg-Marquardt algorithm found that the training process is more efficient than using back-propagation algorithm. Selection of training parameters of the Levenberg-Marquardt algorithm includes the number of hidden layers and the number of nodes in a hidden layer before we can train the neural networks in Matlab environment [*Demuth et al.*, 2006]. As a comparison back-propagation algorithm needs not only those two parameters to be carefully selected, but also other parameters, i.e. momentum and learning rate.

Stand volume was accordingly estimated using field data and remote sensing data as the predictors or the independent variable. The chosen field data was number of stems per sampling plot; as instead of basal area data that have already been used to estimate stand volume, number of stems data are not directly related to the stand volume equation. To some extent, number of stems has the possibility to explain stand volume of a forest, because logically the stand volume per hectare forest area is related to the number of stems in that area for a given age-class or age-class distribution of the forest.

The remote sensing data used to estimate stand volume were surface reflectance of multi-spectral bands (i.e. band 1, 2, 3, 4, 5 and 7 of Landsat 7 ETM+), DEM (i.e. elevation, slope angle and aspect). Vegetation indices calculated from the satellite data, namely Normalized Difference Vegetation Index (NDVI), Simple Ratio (SR), Enhanced Vegetation Index (EVI) and Atmospherically Resistant Vegetation Index (ARVI). Further details on vegetation indices can be found in most remote sensing references [*Jensen*, 1996; *Mather*, 2004; *Richards*, 1993; *Parresol*, 1999].

Above ground biomass prediction

This study estimated the forest biomass through the conversion of the forest stand volume. The above ground biomass was predicted using two equations proposed by Brown and Lugo (1992) [*Fearnside*, 1997]. The Brown and Lugo equation for above ground biomass (AGB_{BL}) is explained as follows:

$$AGB_{(BL)} = SB \cdot BEF \cdot (1 + (0.09 \div 0.21)) \quad \ldots\ldots (7)$$

where *SB* is the stemwood biomass, and is defined by

$$SB = Volume \times VEF \times WD \quad \ldots\ldots (8)$$

with *Volume* ($m^3 \cdot ha^{-1}$) obtained from forest inventory data, *VEF* (volume expansion factor to account for trees smaller than the minimum diameter measured) is 1.25 for dense forests and 1.5 for other than dense forests, *WD* is wood density (0.69 Mg m^{-3} as a weighted average of wood density), and *BEF* (biomass expansion factor to account for biomass in addition to stemwood biomass) varied as a function of stemwood biomass (*SB*) as follows [*Brown* and *Lugo*, 1992].

for $SB < 190$ Mg ha^{-1}, $BEF = e^{[3.213 - 0.506 \cdot \ln(SB)]}$

for $SB > 190$ Mg ha^{-1}, $BEF = 1.74$ ..... (9)

In Eq.(7), $SB \times BEF$ is the conversion of volume to above ground biomass originally proposed by Brown and Lugo (1992). The constants 0.09 and 0.21 in the formula were introduced by [*Huoghton et al.*, 2001] to include below ground biomass and dead above ground biomass.

The second approach for predicting above ground biomass (AGB_{FS}) implemented equation proposed by [*Fearnside*, 1997] that suggested modification of Brown and Lugo Equation (1992):

$$AGB_{(FS)} = SB \times BEF \times (1 + CF) \quad \ldots\ldots (10)$$

where $CF = 96.2\%$, which represents the sum of various correction factors (lianas = 5.3%, trees smaller than 10 cm *DBH* = 12%; tree form factor = 15.6%; trees between 30 and 31.8 cm *DBH* = 3.6%; hollow trees = -6.6%; bark = 0.9%; palms = 2.4%; below ground biomass = 33.6%; dead above ground biomass soil = 31%; and other components = 0.2%) [*Sales et al.*, 2007]. In this study, correction factors from Eq. (7)– Eq. (10) were assumed constant, i.e., not spatially variable.

RESULTS AND DISCUSSION

Spectral response of the corrected satellite image

The surface reflectance of the atmospherically corrected satellite image reveals significant improvement particularly for visible bands (i.e. ETM 1, ETM 2 and ETM 3), as the atmospheric attenuation was minimum for the middle infra red bands, i.e. ETM 5 and ETM 7. Observation on the reflectance value of the uncorrected and atmospherically corrected images was conducted taking samples from some apparent land covers found in the area; the results are exhibited in Figure 2.

Spectral profile of high density forest, road networks, water body and cloud in the study area were taken as samples because we assume the surface reflectance of these land cover types are relatively stable at spatial and temporal scales. The DN values of the visible bands (i.e. ETM 1, ETM 2 and ETM 3) always have higher reflectance as compared to those of partially corrected and atmospherically corrected images. This is due to the DN value being influenced by atmospheric attenuation, topographic conditions and other parameters, such as sun angle, earth-sun distance, etc. Upon comparison with the partially corrected image, we found that DN values have a reduced solar irradiance, sun zenith angle and earth-sun distance effects in NIR and MIR bands (ETM 4, ETM 5 and ETM 7) especially for dark objects (water body and dense forest); but it becomes very noticeable for bright objects (cloud and road networks).

The observation on the partially corrected image found that top of atmosphere (TOA) reflectance corrected only the effects caused by the sun angle, earth-sun distance and the solar radiance, but it ignores the effects of atmospheric scattering. The visible bands are mainly affected by the atmospheric scattering, which provided image additive effects, and this especially occurs for dark objects, e.g. dark vegetation and water body. In contrast, the effects of atmospheric scattering in visible bands are reduced for bright objects, this can be explained from Fig. 2a and Fig. 2c, where the TOA reflectance of road networks and cloud in visible bands have similar values as their surface reflectance.

The atmospheric scattering effects were very low in NIR and MIR bands, both for dark and bright objects. This can be seen in Figure 2 where the partially corrected and atmospherically corrected images show similar values in the NIR and MIR bands. The exceptional case is for water bodies where the reflectance of the partially corrected image in the NIR band is higher than the atmospherically corrected image; this might be due to the suspended sediment matters or water turbidity.

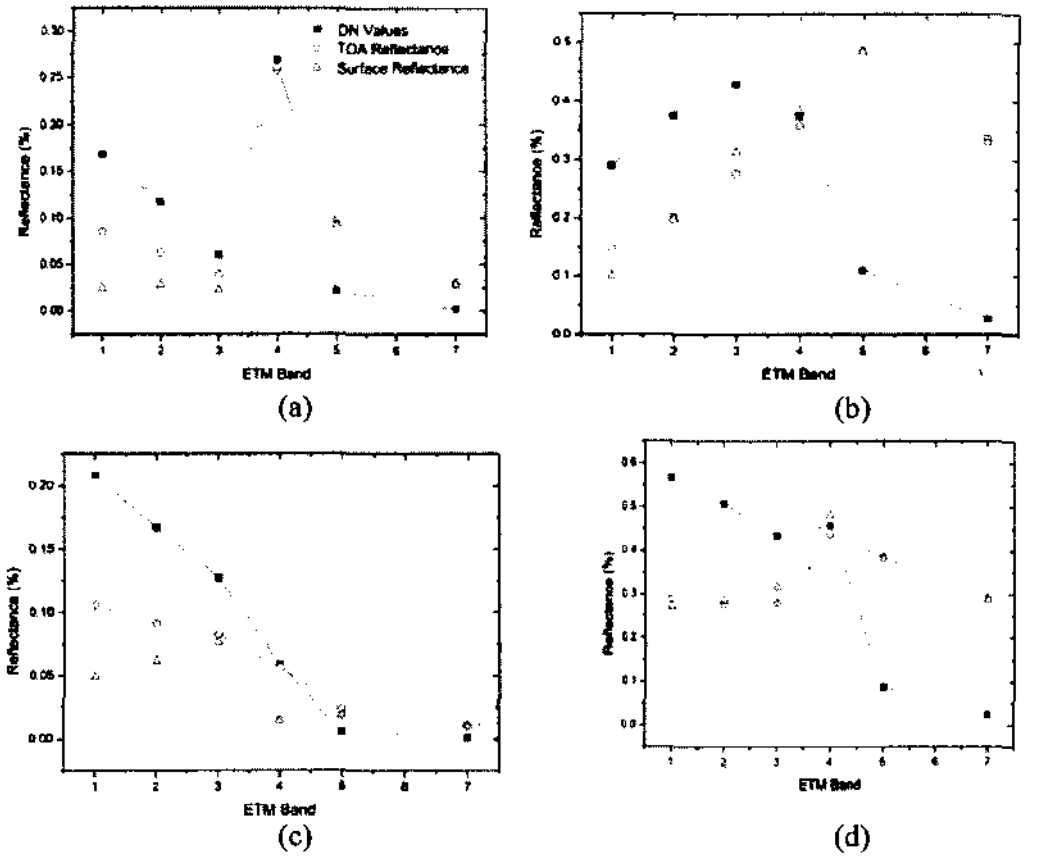

Figure 2. Comparison of corrected and uncorrected spectral responses for different land cover types, namely (a) dense forest, (b) bare soil, (c) water body, and (d) clouds

Prediction of stand volume

Neural networks method applied in this study implemented Levenberg-Marquardt algorithm to train the networks. During training process, the dataset was divided into three subsets, which are training, validation and test datasets.

The training dataset used to train neural networks, while validation is used as a control for training process. When the accuracy of validation data started increasing the training was stopped avoiding overtraining on the networks. Test dataset moreover was used as independent data for assessing the prediction accuracy. Stand volume was estimated using (1) field measurement data (i.e. number of stems per sample plot), (2) remote sensing data (i.e. surface reflectance, DEM, and vegetation indices), and (3) integration of field measurement and remote sensing data. The correlation of predicted and actual stand volume is depicted in Figure 3.

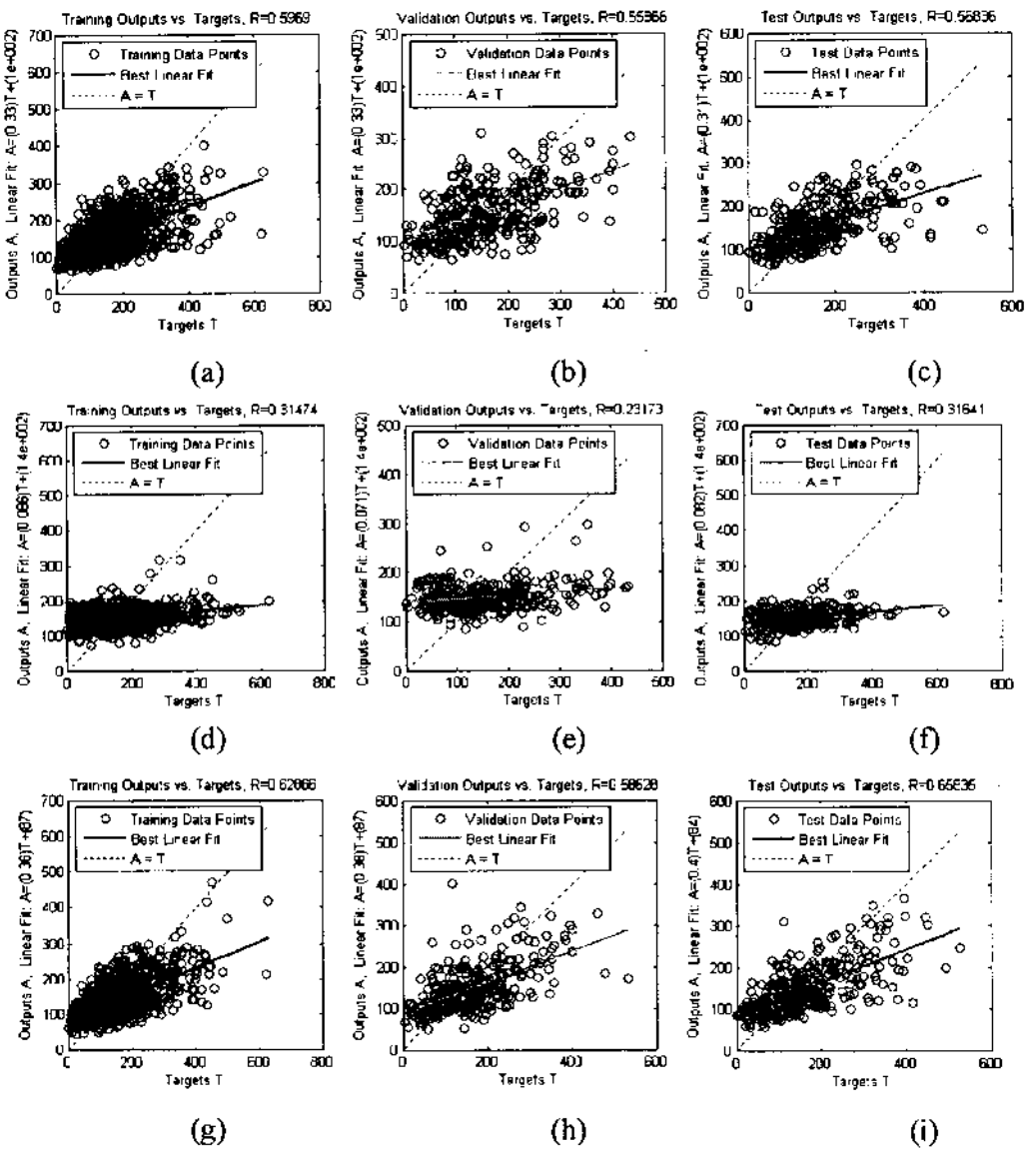

Figure 3. Correlation between predicted and actual stand volume estimated using field data (a, b, c), remote sensing data (d, e, f), and combination of field measurement and remote sensing data (g, h, i)

Correlation coefficient of independent test dataset showed that 31.6% of stand volume can be explained by remote sensing data (Fig. 3f) lower than that predicted using field data (56.8%) (Fig. 3c). Combination of field and remote

sensing data improved the predictive ability of neural networks in estimating stand volume and the correlation between the actual and predicted stand volume increased to 65.8% (Fig. 3i). Although the correlation is statistically acceptable, the volume estimate is underestimated as compared to the field data. This is indicated from the mean estimate, which is 146 m^3/ha, lower than the actual mean volume, which is 159 m^3/ha (Tabel 1).

Table 1. Actual and predicted stand volume estimated using remote sensing image and field data

Actual Stand Volume		Stand Volume Estimate	
Mean	159.1	Mean	146.3
Standard Error	2.4	Standard Error	1.4
Standard Deviation	92.7	Standard Deviation	55.6
Minimum	1.0	Minimum	44.5
Maximum	628.6	Maximum	471.9
Confidence Level(95.0%)	4.7	Confidence Level(95.0%)	2.8

This might be due to the saturation of RS data limiting their ability to assess larger stand volume, i.e. stand volume over 200 m^3/ha. For example, surface reflectance of the corrected image vary from 0.0 to 1.0, and stand volume ranges from 0 – 600 ton/ha. The small interval of surface reflectance caused the correlation with stem volume were compromised, so that the predictive ability of neural networks has less accurate results. Similar with spectral values, NDVI performance is also limited because the indices of green vegetation ranged from 0.7 – 1.0. This condition, so-called saturation or asymptote problem, commonly occurs in satellite data for predicting the biophysical properties of forested lands, resulting in highly scattered correlations at the extreme values of the observed variable.

The coarseness of spatial resolution, i.e. Landsat 7 ETM has 30 meter resolution, is probably another underlying factor responsible for lower correlation and underestimates of the stand volume. One pixel of Landsat ETM data covers 900 m^2 of areas on the ground; with this resolution, variations of forest parameters within single pixel are certainly accumulated. Using a 225 m^2 sample plot, the mixture of different tree compositions is ignored, thus a small error in image registration might cause a huge problem for generating proper correlation with forest properties data. Nevertheless, this study has demonstrated that remote sensing data has potential to improve stand volume estimate coupled with field observation data, i.e. number of stems.

Conversion to above ground biomass

Prediction of the Above Ground Biomass (AGB) was carried out using two equations proposed by [*Brown* and *Lugo*, 1992; *Fearnside*, 1997] converting the values of predicted stand volume. Using Brown and Lugo equation we found mean AGB of 368.33 $Mg.ha^{-1}$, while using Fearnside equation the mean AGB was 555.89 $Mg.ha^{-1}$.

This different result was caused by the conversion factors considered for both equations. Brown and Lugo formula considered only dead above ground- and below ground biomass, whereas Fearnside equation attributed such dead biomasses as well as other adjustment factors of different vegetation types. Histograms of biomass estimates were calculated and the results were depicted on Table 2.

Table 2 Statistics of above ground biomass estimate

AGB (Brown and Lugo)		AGB (Fearnside)
Mean	368.3	555.9
Standard Error	1.8	2.7
Standard Deviation	69.5	104.9
Minimum	214.3	323.5
Maximum	938.9	1417.0
Confidence Level(95.0%)	3.5	5.3

The AGB estimate has higher correlation with number of stems (r = 0.82) compared to stand volume (r = 0.60) and basal area (r = 0.68). Similar with AGB, the stem volume was also underestimated upon comparison with the measured data (Fig. 4). We found relatively weak correlations between forest properties and remote sensing (RS) data, mainly due to highly variable of forest properties values and saturation of RS data. Recent studies have found that simple band ratios are sometimes more useful than complex vegetation indices (e.g. NDVI, SAVI, EVI) for predicting forest stand parameters [*Foody et al.*, 2003; *Lu et al.*, 2004; *Lu*, 2006]. However, we should be careful for selecting satellite band ratios in our study, as these ratios are only sensitive to particular forest properties, so that generalization of those ratios for different applications is rather impossible.

Spatial Distribution of Above Ground Biomass

The AGB estimate was interpolated over the forest concession employing Kriging method assuming spatial correlation of the AGB values. Firstly, the AGB was transformed using log-transform, so that the data was more likely to be normally distributed. Then, the auto-correlation of the AGB values were modeled in semivariogram selecting Gaussian model which best fitted with the spatial

variability of the values. During semivariogram modeling, no special pattern of spatial variability changes within certain direction, so-called anisotropy, was observed, thus omni-directional variogram was considered.

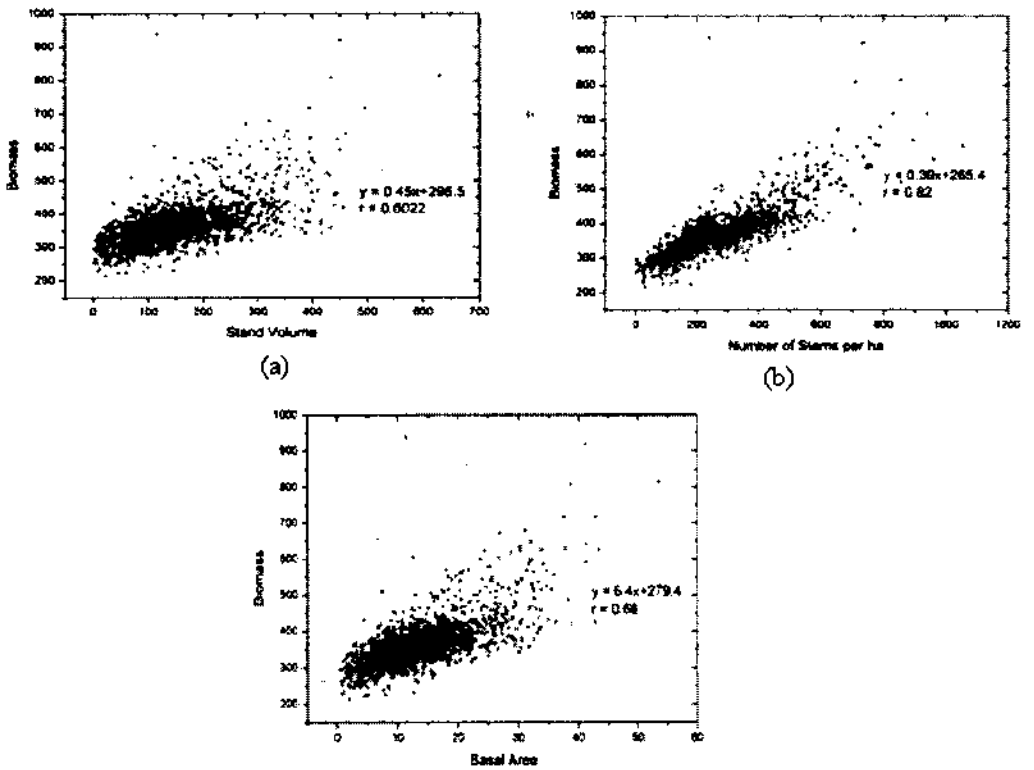

Figure 4. Correlation of AGB estimates with (a) stand volume estimate, (b) basal area, and (c) number of stems

The AGB interpolation was conducted using Ordinary Kriging assuming unknown constant mean of the values over the study area. We assumed spatial correlation was less as the predicted AGB moved further from the sampled locations. Therefore, the interpolation of single pixel considered the neighborhood values within defined distance and directions.

The neighborhood analysis was determined in the NE-SW and NW-SE directions. There were maximum 40 neighboring pixels considered in the interpolation of the unknown value. The neighborhood option has a smoothing effect on the interpolation results (Figure 5a, 5c). The AGB standard error was estimated and we found the error increased as the interpolation was more distant from the sampled area (Figure 5b, 5d). We observed that the transect data has a

systematic error estimate as sampling intensity was concentrated along the central part of the study area. Another sampling technique, like stratified random sampling should be considered to improve the predictive ability of Kriging method.

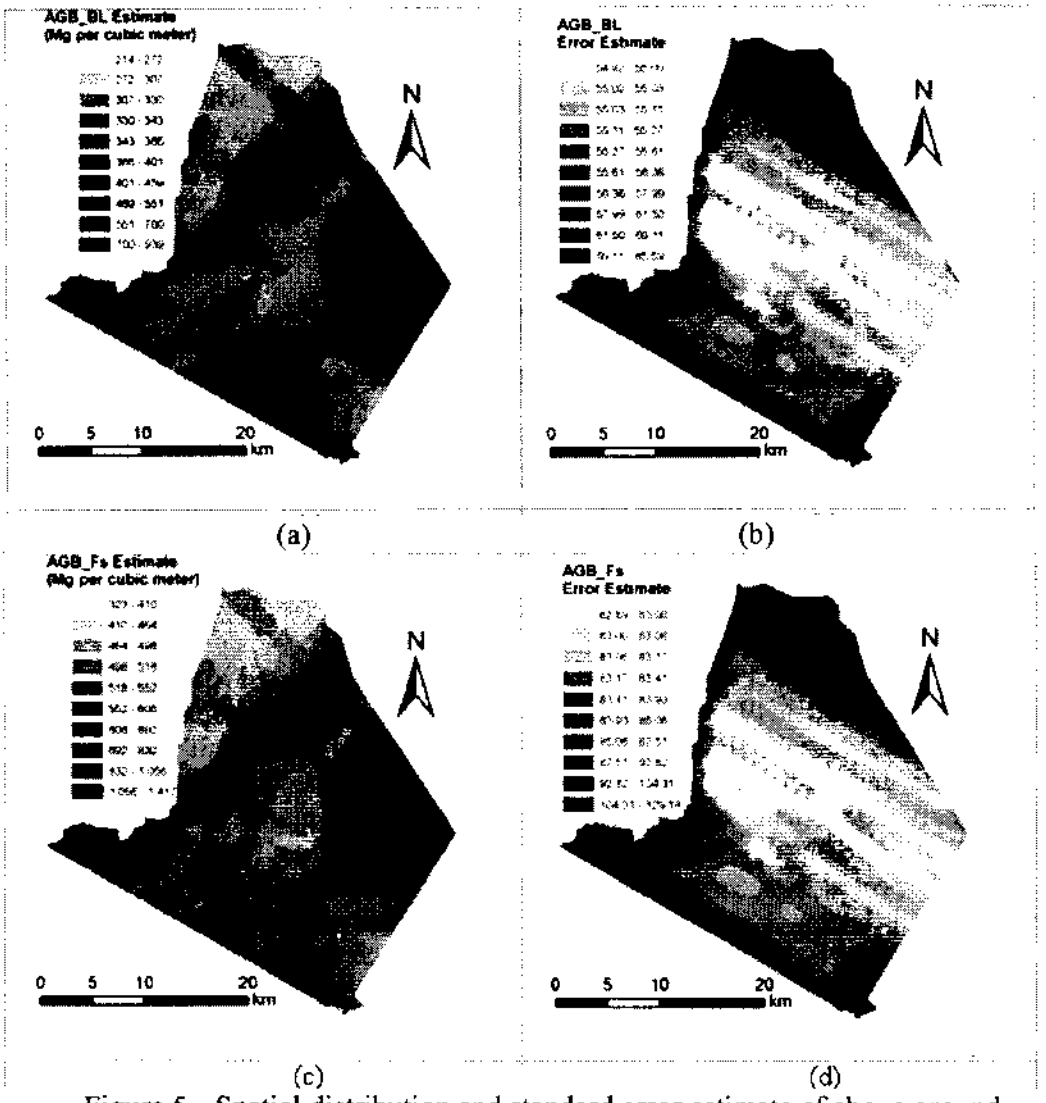

Figure 5. Spatial distribution and standard error estimate of above ground biomass based on Brown and Lugo model (a, b), and Fearnside equation (c, d)

The Fearnside AGB as expected has higher standard error as compared with that of the Brown and Lugo AGB. The earlier has an average standard error of 83.3 Mg/ha while the latter resulted in 55.19 Mg/ha of the average standard error. This is due to the Fearnside equation estimated higher above ground biomass over the

study area. According to the kriging interpolation results, the Fearnside and the Brown and Lugo equations estimated in average 555.53 Mg/ha and 368.06 Mg/ha, respectively. There is no significant difference between the AGB estimated from the conversion of the stand volume with that resulted from the kriging interpolation.

The interpolation using kriging has a major drawback, which is less robust than the simple procedure of the conversion of stand volume data. The kriging interpolation requires a large number of parameters, namely the type of variogram model (e.g. spherical, exponential, and Gaussian), variogram parameters (e.g. nugget, sill, and range) and the choice of kriging method.

There are different kriging methods that can be employed for spatial prediction of un-sampled areas, like ordinary kriging, simple kriging and kriging with a trend model. Different assumptions regarding to data distribution and type should be initially formulated for selecting the right choice of kriging method applied for data interpolation. The main advantage of the kriging interpolation is that one can study spatial distribution of the predicted variable, i.e. above ground biomass, and the interpolation results can give more information of such variable.

CONCLUSION

The dark object subtraction (DOS) method demonstrated in this study found that the NIR and MIR bands were less affected by the atmospheric scattering effects. This technique has efficiently corrected the sun zenith angle, solar irradiance, and earth-sun distance effects. Stand volume estimated from Levenberg-Marquardt neural networks found 146 m^3/ha of mean volume in the study area, slightly lower than the measured data (159 m^3/ha). Combination of remote sensing data, i.e. spectral data, vegetation indices and DEM, and field data, i.e. number of stems, had higher correlation coefficient with the observed stand properties compared to the individual use of those input data. The AGB's assessed from stand volume resulted in different estimates mainly due to various adjustment factors. The AGB predicted using Brown – Lugo equation varied from 214 to 939 $Mg.ha^{-1}$, while Fearnside model, including additional adjustment components, estimated 323 to 1417 $Mg.ha^{-1}$ of AGB. Spatial distribution of the AGB found higher standard error in lower sampling intensity areas.

REFERENCES

Atkinson, P.M. and A.R.L. Tatnall (1997), Introduction Neural networks in remote sensing. *International Journal of Remote Sensing, 18*, 699-709.

Austin, J., B. Mackey and K. VanNiel (2003), Estimating forest biomass using satellite radar: an exploratory study in a temperate Australian Eucalyptus forest. *Forest Ecology & Management, 176*, 575 - 583.

Baik, J.-J. and J.S. Paek (2000), A neural network model for predicting typhoon intensity. *Journal of the Meteorological Society of Japan, 78*, 857-869.

Berry, W.D. and S. Feldman (1985), *Multiple Regression in Practice*. Sage, Newbury Park, CA.

Bolanca, T., S. Cerjan-Stefanovic and M. Novic (2005), Application of Artificial Neural Network and Multiple Linear Regression Retention Models for Optimization of Separation in Ion Chromatography by Using Several Criteria Functions. *Chromatographia, 61*, 181-187.

Brown, S. and A.E. Lugo (1992), Aboveground biomass estimates for tropical moist forests of the Brazilian Amazon. *Interciencia, 17*, 8-18.

Chavez Jr., P.S. (1988), An Improved Dark-Object Subtraction Technique for Atmospheric Scattering Correction of Multispectral Data. *Remote Sensing of Environment, 24*, 459-479.

Chavez Jr., P.S. (1996), Image-based atmospheric corrections - Revisited and improved. *Photogrammetric Engineering and Remote Sensing, 62*, 1025-1036.

Cohen, J. and P. Cohen. (1983), *Applied multiple regression/correlation analysis for the behavioral sciences* Lawrence Erlbaum Associates, Inc., Hillsdale, NJ.

DeGier, A. (2003), A new approach to woody biomass assessment in woodlands and shrublands. In *Geoinformatics for Tropical Ecosystems* (ed P. Roy), 161-198, India.

Demuth, H., M. Beale and M. Hagan (2006), Neural Network Toolbox 5 *User's Guide* The MathWorks, Inc., Apple Hill Drive Natick, MA.

Fearnside, P.M. (1997), Greenhouse gases from deforestation in Brazilian Amazonia: Net committed emissions. *Climatic Change, 35*, 321-360.

Foody, G.M., D.S. Boyd and M.E.J. Cutler (2003), Predictive relations of tropical forest biomass from Landsat TM data and their transferability between regions. *Remote Sensing of Environment, 85*, 463-474.

Foody, G.M. and D.P. Cox (1994), Sub-pixel land cover composition estimation using a linear mixture model and fuzzy membership functions. International *Journal of Remote Sensing, 15*, 619-631.

Hagan, M.T. and M.B. Menhaj (1994), Training feedforward networks with the Marquardt algorithm. Neural Networks, *IEEE Transactions on, 5*, 989-993.

Houghton, R.A., K.T. Lawrence, J.L. Hackler and S. Brown (2001), The spatial distribution of forest biomass in the Brazilian Amazon: A comparison of estimates. *Global Change Biology, 7*, 731-746.

Jensen, J.R. (1996), *Introductory Digital Image Processing*: A remote Sensing Perspective, Second Edition. Prentice Hall.

Landsat Project Science Office (1998), Landsat 7 Science *Data Users Handbook*, Vol. 2007. NASA's Goddard Space Flight Center, Greenbelt, Maryland.

Lefsky, M.A., W.B. Cohen,D.J. Harding, G.G. Parker, S.A. Acker and S.T. Gower (2002), Lidar remote sensing of above-ground biomass in three biomes. *Global Ecology and Biogeography, 11*, 393-399.

Lim, C.W. and T. Kirikoshi (2005), Prediction of Promotional Effect Using Neural Network Modeling. *Journal of Pharmaceutical Marketing and Management, 16*, 3-26.

Losi, C.J., T.G. Siccama, R. Condit and J.E. Morales (2003), Analysis of alternative methods for estimating carbon stock in young tropical plantations. *Forest Ecology and Management, 184*, 355-368.

Lu, D., P. Mausel, E. Brondizio and E. Moran (2004), Relationships between forest stand parameters and Landsat TM spectral responses in the Brazilian Amazon Basin. *Forest Ecology and Management, 198*, 149-167.

Lu, D.S. (2006) The potential and challenge of remote sensing-based biomass estimation. *International Journal of Remote Sensing, 27*, 1297-1328.

Mantel, S. (1998), *Soil and Terrain of the Labanan Area:* Development of an environmental framework for the Berau Forest Management Project. Berau Forest Management Project, Berau.

Mather, P.M. (2004), *Computer Processing of Remotely-Sensed Data*: An Introduction, Third Edition edn. John Wiley & Sons, Ltd, Chichester, West Sussex.

Minnaert, M. (1941), The reciprocity principle in lunar photometry. *Astrophysical Journal, 93*, 403-410.

Parresol, R. (1999), Assessing Tree and Stand Biomass: A Review with Examples and Critical Comparisons. *Forest Science, 45*, 573-593.

Rahman, M.M., E. Csaplovics and B. Koch (2005), An efficient regression strategy for extracting forest biomass information from satellite sensor data. *International Journal of Remote Sensing, 26*, 1511-1519.

Rauste, Y. (2005), Multi-temporal JERS SAR data in boreal forest biomass mapping. *Remote Sensing of Environment, 97*, 263-275.

Riaño, D., E. Chuvieco, J. Salas and I. Aguado (2003), Assessment of Different Topographic Corrections in Landsat-TM Data for Mapping Vegetation Types. *IEEE Transactions on Geoscience and Remote Sensing, 41*, 1056 - 1061.

Richards, J.A. (1993), *Remote Sensing Digital Image Analysis - An Introduction*, Second Edition, Springer-Verlag, New York.

Sales, M.H., C.M. Souza Jr., P.C. Kyriakidis, D.A. Roberts and E. Vidal (2007), Improving spatial distribution estimation of forest biomass with geostatistics: A case study for Rondonia, Brazil. *Ecological Modelling, 205*, 221-230.

Sathe, P.M. and J. Venitz (2003), Comparison of Neural Network and Multiple Linear Regression as Dissolution Predictors. *Drug Development and Industrial Pharmacy, 29*, 349 - 355.

Schroeder, T.A., W.B. Cohen, C. Song, M.J. Canty and Z. Yang (2006), Radiometric correction of multi-temporal Landsat data for characterization of early successional forest patterns in western Oregon. *Remote Sensing of Environment, 103*, 16-26.

Song, C., C.E. Woodcock, K.C. Seto, M.P. Lenney and S.A. Macomber (2001), Classification and change detection using Landsat TM data: When and how to correct atmospheric effects? *Remote Sensing of Environment, 75*, 230-244.

Sousa, S.I.V., F.G. Martins, M.C.M. Alvim-Ferraz and M.C. Pereira (2007), Multiple linear regression and artificial neural networks based on principal components to predict ozone concentrations. *Environmental Modelling and Software, 22*, 97-103.

Teillet, P.M., B. Guindon and D.G. Goodenough (1982), On the slope-aspect correction of multispectral scanner data. *Canadian Journal of Remote Sensing, 8*, 84-106.

Wijaya, A. (2006), Comparison of soft classification techniques for forest cover mapping. *Journal of Spatial Science, 51*, 7-18.